JOURNAL OF SOLID STATE CHEMISTRY **127,** 169–177 (1996)
ARTICLE NO. 0373

Sample Dependence of Magnetic Properties and Determination of Antiferromagnetic Structure of $NdPd_2Al_3$

A. Dönni,* H. Kitazawa,† P. Fischer,* T. Vogt,‡ A. Matsushita,† Y. Iimura,§ and M. Zolliker*,[1]

*Laboratory for Neutron Scattering, ETH Zürich and Paul Scherrer Institute, CH-5232 Villigen PSI, Switzerland; †National Research Institute for Metals, Tsukuba, Ibaraki 305, Japan; ‡Physics Department, Brookhaven National Laboratory, Upton, New York 11973; and §Institute of Physical and Chemical Research (RIKEN), Wako, Saitama 351-01, Japan

Received April 30, 1996; accepted August 22, 1996

For the ternary intermetallic compound $NdPd_2Al_3$ systematic measurements by means of X-ray diffraction, dc susceptibility, and specific heat on a series of polycrystalline and single-crystalline samples reveal a significant dependence of physical and magnetic properties on sample preparation procedures. The Néel temperature T_N with values between 7.7 K and 5.2 K shows a linear dependence on the hexagonal lattice constant a, which is not valid for c. The best $NdPd_2Al_3$ sample was investigated by high-resolution powder neutron diffraction: The crystal structure agrees well with the ordered hexagonal $PrNi_2Al_3$-type structure. The antiferromagnetic structure corresponds to a propagation vector $\mathbf{k} = [1/2, 0, 0]$. The ordered magnetic Nd moments of $(2.28 \pm 0.07)\ \mu_B$ at saturation lie in the basal plane due to the crystal–electric field anisotropy and are oriented perpendicular to the propagation vector. Magnetic properties of $NdPd_2Al_3$ are compared with those of isostructural compounds including the heavy-fermion superconductor UPd_2Al_3 and the heavy-fermion antiferromagnetic $CePd_2Al_3$.

1. INTRODUCTION

Discovery of the heavy-fermion superconductor UPd_2Al_3 (1) ($\gamma = 150$ mJ K^{-2} mol^{-1}, $T_c = 2$ K, $T_N = 14$ K), in which superconductivity coexists with a large antiferromagnetically ordered uranium moment of 0.85 μ_B (2), has stimulated the exploration of magnetic properties of related isostructural lanthanide compounds $REPd_2Al_3$. The compound with RE = Ce (3–6) has been studied in detail, whereas only limited information is available so far concerning RE = Pr (7), Nd (7), Sm (7, 8), and Gd (9).

UPd_2Al_3 adopts the hexagonal $PrNi_2Al_3$-type crystal structure shown in Fig. 1 with room temperature lattice parameters $a = 5.365$ Å and $c = 4.186$ Å. This crystal structure consists of layers of U and Pd atoms, alternating along the c direction with layers of pure Al. The magnetic structure corresponds to a ferromagnetic coupling in the magnetically easy ab plane and an antiferromagnetic stacking along the magnetically hard c axis with a magnetic propagation vector $\mathbf{k} = [0, 0, 1/2]$. For UPd_2Al_3 superconducting and magnetic properties depend on sample preparation. Polycrystalline samples are usually prepared by arc-melting stoichiometric amounts of the constituents, and single-crystalline samples are then obtained by the Czochralsky pulling method. Sato *et al.* (10, 11) observed that single-crystalline UPd_2Al_3 has a lower superconducting transition temperature T_c and a higher residual electrical resisitivity than polycrystalline UPd_2Al_3. This effect, which can be ascribed to the evaporation of aluminum during the process of sample preparation, can be partly compensated by varying the composition of the starting material. For an $UPd_2Al_{3.03}$ single crystal, prepared by using 1% excess aluminium, the residual electrical resistivity (11) was reduced from the higher value of the UPd_2Al_3 single crystal down to the lowest value of polycrystalline UPd_2Al_3 samples. Furthermore, the transition width ΔT_c of single-crystalline $UPd_2Al_{3.03}$ was substantially smaller than that of single-crystalline UPd_2Al_3. The $PrNi_2Al_3$-type crystal structure is completely ordered, so that within this space group, there is no possibility of interchange of U and Pd atoms, nor any position for extra Al atoms. X-ray diffraction measurements (12) of single crystals prepared with starting U:Pd:Al compositions of 1:2:3.03 and 1:2:3.06 revealed no evidence for a deviation from $PrNi_2Al_3$-type long-range ordering in this material. The refinement, which was not sensitive to the Al stoichiometry (±10%), excluded any appreciable exchange between U and Pd atoms. More sensitive synchrotron X-ray back-reflection Laue photographs (12) obtained on the same samples presented evidence for some short-range disorder (either interstitial Al atoms or defects in the Al layer) in the direction parallel to the hexagonal c axis. Concerning the second-order antiferromagnetic phase transition, the sample dependence of the Néel temperature $T_N = 14.3$ K is weak; however, for UPd_2Al_3 single crystals, a small anomaly in the order pa-

[1] Present address: Institut Laue-Langevin, BP136, F-38042 Grenoble, France.

0022-4596/96 $18.00

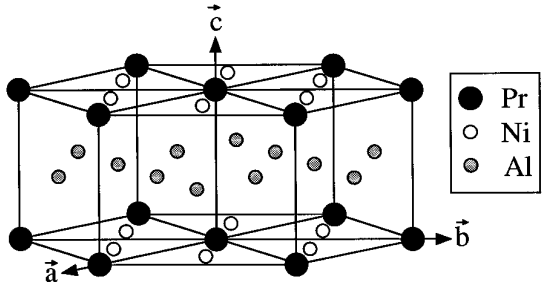

FIG. 1. $PrNi_2Al_3$-type crystal structure. Hexagonal space group $P6/mmm$ with sites ($1a$) occupied by Pr, ($2c$) by Ni, and ($3g$) by Al.

rameter near 12 K, which indicates an additional first-order phase transition, has been observed by magnetic susceptibility (13), resonant magnetic X-ray scattering (14), and neutron diffraction (15). For polycrystalline UPd_2Al_3 samples neutron diffraction experiments (2, 16) revealed enormously large preferred orientation effects and the evolution of a second incommensurate magnetic phase with a propagation vector $\mathbf{k}_2 \approx [0, 0, 0.52]$ for increasing temperature.

The nonsuperconducting cerium homolog $CePd_2Al_3$ may be characterized (3, 17) as a heavy-fermion antiferromagnet (γ = 380 mJ K^{-2} mol^{-1}, T_N = 2.8 K), which is located very close to the magnetic-to-nonmagnetic boundary in the Kondo-lattice phase diagram. The occurrence of magnetic ordering critically depends on the exact occupation and distribution of aluminum atoms over their available lattice sites (5). For well-prepared polycrystalline material of $CePd_2Al_3$, characterized by small lattice constants, long-range antiferromagnetic ordering with a cerium moment of 0.47(2) μ_B at saturation (4) appears below T_N = 2.8 K. Further polycrystalline $CePd_2Al_3$ samples prepared by a splat cooling technique (17) as well as single-crystalline $CePd_2Al_3$ samples (5) show a higher degree of structural disorder, and no long-range magnetic ordering is observed in the measured temperature range down to 1.8 and 0.4 K, respectively.

In this paper we address the investigation of magnetic properties of the metallic Kramer's doublet system $NdPd_2Al_3$, which is a stable $4f$ moment analog of $CePd_2Al_3$. A series of selected polycrystalline and single-crystalline $NdPd_2Al_3$ samples, prepared with two different starting compositions, have been systematically investigated by measurements of X-ray diffraction, dc susceptibility, and specific heat to establish the correlations between sample preparation procedure, crystal perfection (room temperature lattice parameters), and magnetic properties (Néel temperature). Crystal and antiferromagnetic structures of $NdPd_2Al_3$ were refined from high-resolution powder neutron diffraction data obtained on the best $NdPd_2Al_3$ sample. Magnetic properties of $NdPd_2Al_3$ are compared with those of isostructural compounds including the heavy-fermion superconductor UPd_2Al_3 and the heavy-fermion antiferromagnet $CePd_2Al_3$.

2. EXPERIMENTAL

Polycrystalline (PC) samples were synthesized by arc-melting the pure elements (Nd:3N, Pd:4N, Al:5N) with two different starting Nd:Pd:Al compositions of 1:2:3 (stoichiometric) and 1:2:3.03 (aluminum-rich) in an argon atmosphere under continuous titanium gettering. The samples were melted several times by turning over each time until a homogeneous button was formed. The average weight loss during melting was 0.13 and 0.17% for stoichiometric and aluminum-rich $NdPd_2Al_3$ samples, respectively. Single-crystal (SC) samples were then prepared from a melt of an aluminum-rich sample in the same triarc furnace by the Czochralsky pulling method. Some samples were annealed at 900°C for 120 h in high vacuum. Starting compositions and heat treatment conditions of five selected $NdPd_2Al_3$ samples (PC1, PC1a, PC2, SC2, SC2a) are given in Table 1. It should be noted that starting compositions are nominal compositions at the beginning of the material production. The compositions of the final $NdPd_2Al_3$ samples, which were not determined, are likely to be slightly changed because of the different vapor pressures of the constituents. For example, a hypothetical evaporation of 1% excess aluminum in an aluminum-rich sample gives rise to a weight reduction of 0.18%, which is comparable to the experimentally observed weight loss.

Room temperature lattice parameters of the $NdPd_2Al_3$ samples were determined by the X-ray whole-pattern decomposition method (18). As internal standard, commercially available high-purity silicon powder (a = 5.430940(35) Å at 298.1 K; Standard Reference Material No. 640b, National Bureau of Standards, Gaithersburg, MD) was used. The magnetic dc susceptibility $\chi \equiv M/H$ of powdered pieces of the $NdPd_2Al_3$ samples was measured

TABLE 1
Characterization of Selected $NdPd_2Al_3$ Samples[a]

Sample	Starting composition Nd:Pd:Al	Heat treatment	a (Å)	c (Å)	T_N (K)
PC1	1:2:3	900°C/120 h	5.4419 (1)	4.2069 (1)	7.7 (1)
PC1a	1:2:3	As cast	5.4432 (1)	4.2092 (1)	6.5 (2)
PC2	1:2:3.03	900°C/120 h	5.4426 (1)	4.2078 (1)	7.2 (1)
SC2	1:2:3.03	900°C/120 h	5.4449 (1)	4.2094 (1)	5.3 (2)
SC2a	1:2:3.03	As grown	5.4451 (1)	4.2093 (1)	5.2 (2)

[a] a, c, Room temperature lattice parameters; T_N, average Néel temperature corresponding to the maximum of the anomaly of the magnetic susceptibility (see Fig. 2a).

down to 1.8 K in an external field of 0.1 T by using a SQUID magnetometer (Quantum design). Specific heat experiments were performed for samples PC1 and PC1a between 1.5 and 25 K by an adiabatic heat pulse method.

A large amount (18 g) of the best $NdPd_2Al_3$ sample (PC1) was investigated on the high-resolution neutron powder diffractometer (HRPD) (19, 20) with 64 detectors at Brookhaven National Laboratory, Upton, New York. The sample was filled under a helium gas atmosphere into a cylindrical vanadium container of 10 mm diameter and mounted in a standard ^{4}He ILL-type cryostat. The neutron wavelength $\lambda = (1.886 \pm 0.001)$ Å was obtained from a vertically focused germanium (511) wafer monochromator. Diffraction data were collected with a primary collimation of 11 min in the paramagnetic state at 14 K and in the magnetically ordered state at 1.5 K. In this configuration the HRPD spectrometer attains a high resolution of $\Delta d/d = 9.7 \times 10^{-4}$ near the take-off angle $2\theta = 120°$, where d is the interplanar lattice spacing. The temperature dependence of the magnetic structure of the same PC1 sample was investigated in an additional neutron diffraction experiment at Institute Laue Langevin, Grenoble, France. The triple-axis spectrometer IN3 was operated in the two-axis mode by using a neutron wavelength $\lambda = 2.36$ Å, a 92 mm pyrolythic graphite filter, and collimations of 40 min/30 min in front of and behind the sample.

3. RESULTS AND DISCUSSION

3.1. Sample Dependence of Magnetic Properties

The X-ray diffraction patterns of all five $NdPd_2Al_3$ samples can be completely indexed with the hexagonal $PrNi_2Al_3$-type structure, and traces of possible impurity phases are limited to well below 1% of the observed total Bragg intensities. The refined room temperature lattice parameters, listed in Table 1, show a significant sample dependence with differences of up to 0.0032(2) Å for a and 0.0025(2) Å for c.

The magnetic susceptibility χ of $NdPd_2Al_3$ is reported (7) to follow a Curie–Weiss law at high temperatures (100 K $< T <$ 300 K) with an effective magnetic moment $\mu_{eff} = 3.6\ \mu_B$, which is close to the free ion value of 3.62 μ_B for the $^4I_{9/2}$ ground state J multiplet of Nd^{3+} ions. Figure 2a shows the low-temperature part ($T < 24$ K) of χ for powdered pieces of the five $NdPd_2Al_3$ samples. The maximum in χ, which appears at the antiferromagnetic phase transition, shows again an essential sample dependence with average Néel temperatures T_N between 7.7 and 5.2 K. $NdPd_2Al_3$ samples with a higher value for T_N (PC1, PC2) have smaller lattice parameters, and the sharp maximum in the susceptibility (see Fig. 2a) indicates that the magnetic phase transition is well defined in the sample. $NdPd_2Al_3$ samples with a lower value for T_N (SC2, SC2a) have larger lattice parameters and the broad maximum of χ reveals

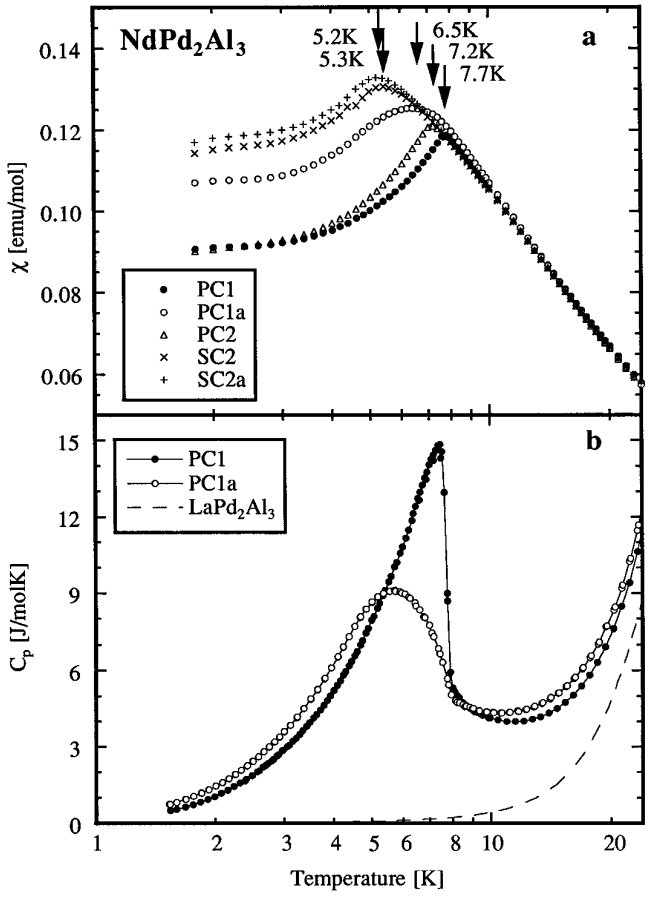

FIG. 2. Temperature dependence of (a) magnetic susceptibility χ and (b) specific heat C_p for selected $NdPd_2Al_3$ samples below 24 K. Specific heat data of the nonmagnetic reference system $LaPd_2Al_3$ are taken from Ref. (8).

that the magnetic phase transition corresponds to a distribution of different transition temperatures within the sample. The smaller the values for the lattice parameters, the higher is the degree of structural perfection with respect to the ideal $PrNi_2Al_3$-type lattice. Effects of site disorder and/or vacancies affect the magnetic exchange interactions in $NdPd_2Al_3$ and shift the onset of long-range magnetic order to lower temperatures. Plots of the room temperature lattice parameters a and c versus the Néel temperature T_N are displayed in Fig. 3. For $NdPd_2Al_3$ we find that the Néel temperature shows a linear dependence on the lattice parameter a, which is not valid for c. This means that magnetism in $NdPd_2Al_3$ is dominated by exchange interactions inside the hexagonal ab plane.

For $NdPd_2Al_3$ the correlations between sample preparation procedure and sample quality (defined as structural perfection) may be summarized as follows:

1. PC samples have generally higher quality than SC samples.

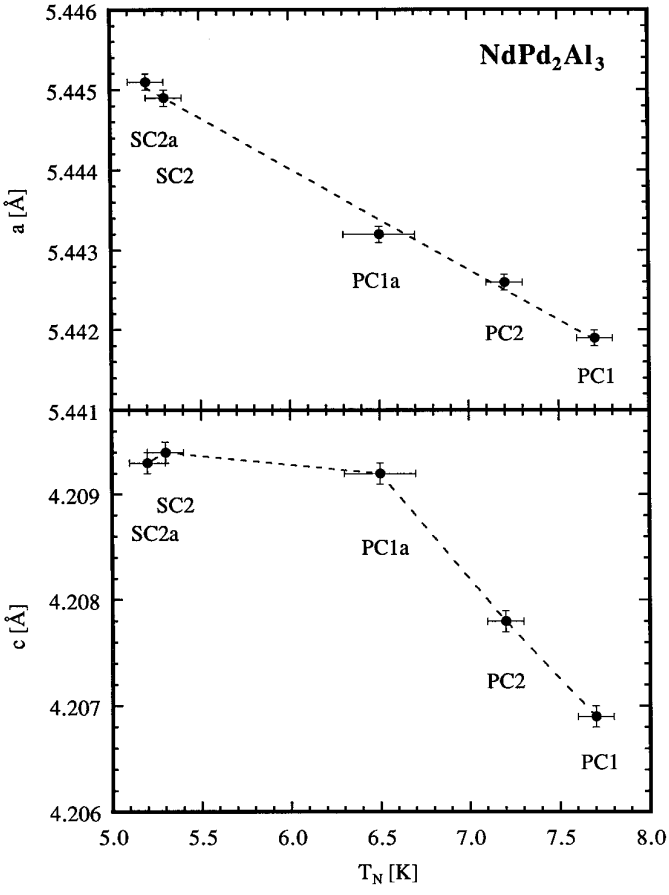

FIG. 3. Room temperature lattice parameters a and c versus Néel temperature T_N for different $NdPd_2Al_3$ samples.

2. Annealing a PC sample produces an essential improvement in quality.

3. Annealing a SC sample leads to a small improvement in quality.

4. The quality of the PC1 sample (prepared with a stoichiometric starting composition) is slightly higher than that for the PC2 sample (prepared with a nonstoichiometric starting composition).

During the process of sample preparation the $NdPd_2Al_3$ material is exposed for a certain time to evaporation of mainly aluminum. This time is about 2 min for the higher-quality PC samples compared with about 6 h for the lower-quality SC samples. An annealing process does essentially improve the structural perfection of PC samples, whereas it cannot compensate anymore for the larger material loss of SC samples. We mention that the value $T_N = 6.5$ K of the polycrystalline $NdPd_2Al_3$ sample of Ref. (7), which is reported to be annealed at 900°C similar to our samples PC1 ($T_N = 7.7$ K) and PC2 ($T_N = 7.2$ K), is surprisingly low and matches the value $T_N = 6.5$ K observed for our as-cast sample PC1a.

Figure 2b shows the specific heat below 24 K for $NdPd_2Al_3$ samples PC1 (annealed) and PC1a (as cast). The shape of the specific heat anomaly at the magnetic phase transition is dramatically altered between the two materials. For the PC1 sample the almost λ-type C_p anomaly is close to what one expects for a high-quality substance with a second-order phase transition at $T_N = 7.7$ K, whereas the C_p anomaly of the lower-quality sample PC1a appears with a reduced height and a broadened width. The magnetic part of the specific heat, C_{mag}, was determined from the difference in specific heats of $NdPd_2Al_3$ and of the nonmagnetic reference system $LaPd_2Al_3$. Figure 4 shows the temperature dependence of C_{mag}/T and of the magnetic entropy S_{mag}/R, obtained by integrating C_{mag}/T, for the two samples PC1 and PC1a. The tenfold degenerate ground-state J multiplet $^4I_{9/2}$ of the magnetic Nd^{3+} ion is split by the crystalline electric field (CEF) interaction of hexagonal symmetry into five doublets (Γ_7, $\Gamma_8^{(1)}$, $\Gamma_8^{(2)}$, $\Gamma_9^{(1)}$, $\Gamma_9^{(2)}$). For both samples the magnetic entropy S_{mag} reaches the value $R \cdot \ln 2$ (of the CEF ground-state doublet) below the respective Néel temperatures and the value $R \cdot \ln 4$ (of two CEF doublets) below 20 K. Thus, in $NdPd_2Al_3$ the energy separation of the two lowest-lying CEF doublets is comparable to the Néel temperature. This was confirmed in an inelastic neutron scattering experiment (21), which yielded a CEF level sequence of $\Gamma_7 \rightarrow \Gamma_9^{(1)} \rightarrow \Gamma_8^{(1)} \rightarrow \Gamma_8^{(2)} \rightarrow \Gamma_9^{(2)}$ for increasing energy transfer and a $\Gamma_7 \rightarrow \Gamma_9^{(1)}$ transition of 10 K.

3.2. Determination of Antiferromagnetic Structure

The HRPD powder neutron diffraction pattern of $NdPd_2Al_3$ (sample PC1) in its paramagnetic state at 14 K is shown in Fig. 5a. The observed intensity distribution

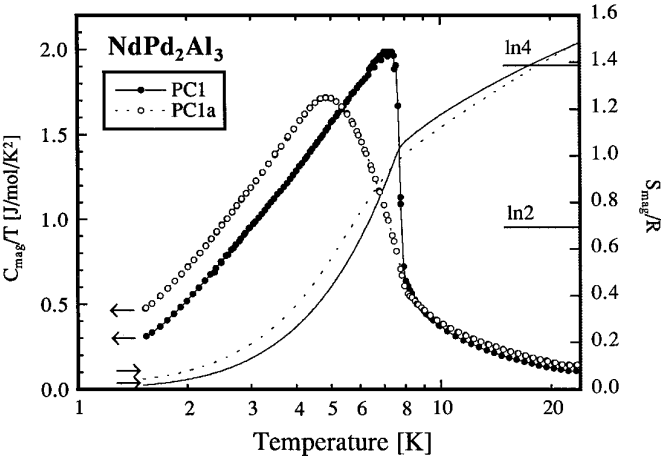

FIG. 4. Temperature dependence of magnetic part of specific heat divided by T, C_{mag}/T, and magnetic entropy S_{mag}/R for selected $NdPd_2Al_3$ samples below 24 K. The contributions to S_{mag}/R below 1.65 K were estimated as 0.018 (PC1) and 0.044 (PC1a).

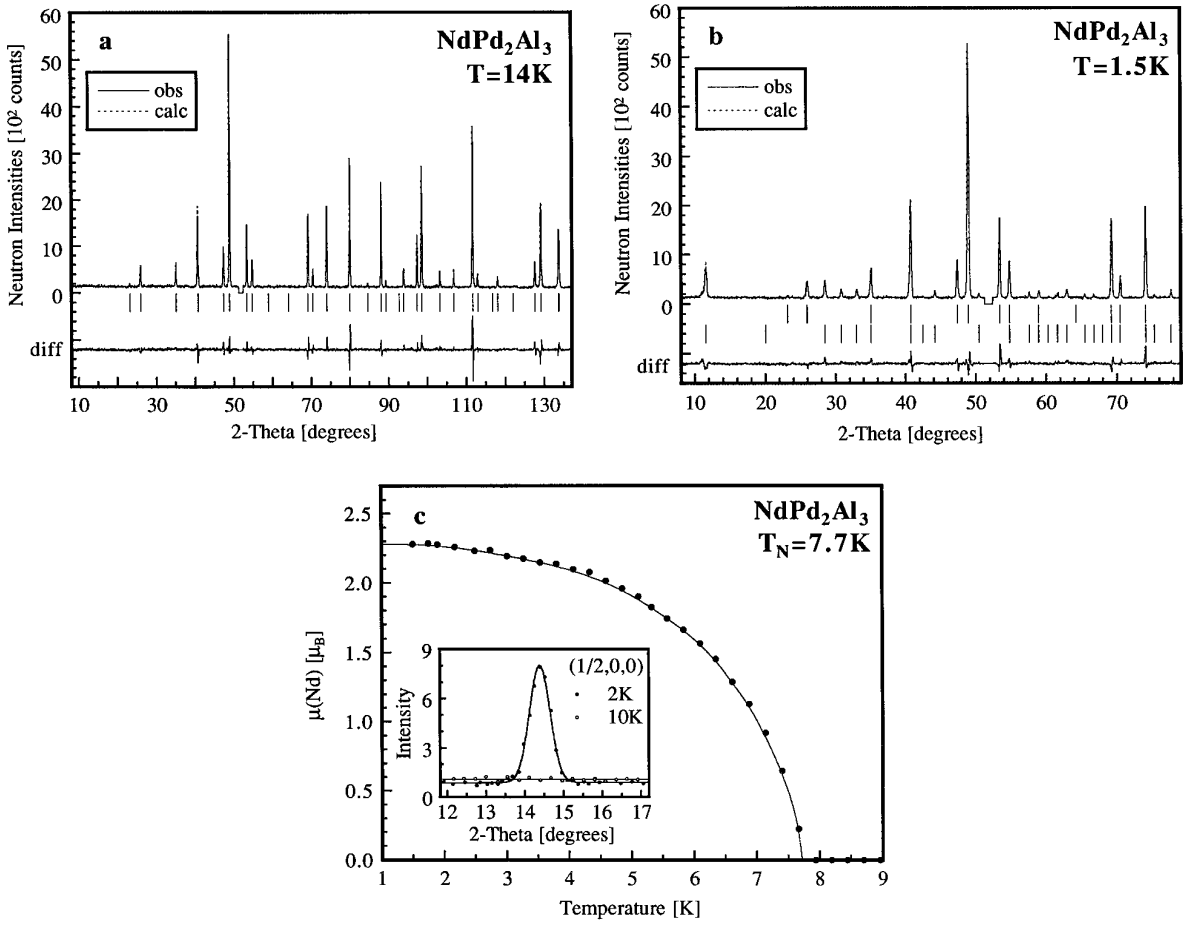

FIG. 5. Observed, calculated, and difference HRPD (BNL) neutron diffraction patterns ($\lambda = 1.886$ Å) of (a) paramagnetic $NdPd_2Al_3$ at 14 K and (b) magnetically ordered $NdPd_2Al_3$ at 1.5 K. The scattering angle region $51.3° < 2\theta < 52.3°$ was excluded from the fits because of a weak Bragg peak from the vanadium sample container. Vertical bars indicate positions of Bragg peaks from crystal and magnetic structures, respectively. (c) Temperature dependence of the ordered magnetic Nd moment based on the observed neutron intensities of the (1/2, 0, 0) reflection of $NdPd_2Al_3$ (see inset).

corresponds to a ternary compound possessing the hexagonal $PrNi_2Al_3$-type structure [space group $P6/mmm$ with Nd on the (1a) sites, Pd on the (2c) sites, and Al on the (3g) sites]. A total of 37 inequivalent nuclear Bragg reflections in the scattering angle range $8° \leq 2\theta \leq 137°$ were refined by the program FullProf (22), including a fit of the background represented by a self-adjusting polynomial. The resulting structural parameters for $NdPd_2Al_3$ at 14 K are given in Table 2. Calculated and observed integrated neutron intensities are compared in Table 3. The FullProf refinement, based on the neutron scattering lengths (in units of 10^{-12} cm) of 0.769 (Nd), 0.591 (Pd), and 0.3449 (Al) (23), finally converged to the agreement values $R_{wp} = 12.5\%$ and $R_{I,N} = 5.39\%$, concerning weighted and integrated intensities, respectively. From counting statistics, the expected value was $R_{exp} = 7.04\%$, yielding $\chi^2 = (R_{wp}/R_{exp})^2 = 3.13$. In the difference pattern of Fig. 5a small deviations between observed and calculated peak positions, which appear in opposite directions for the strong nuclear Bragg peaks (3, 0, 1) at $2\theta = 79.9°$ and (2, 2, 2) at $2\theta = 111.6°$ (see Fig. 5a), are caused by the instrumental peak shape of the HRPD spectrometer, because the detector height ($H = 10$ cm) is large compared with the distance from sample to detector ($L = 99$ cm) (24). Similar effects were observed in the HRPD diffraction pattern of a reference sample (cubic CeO_2). Based on the absence of major disagreements between observed and calculated integrated peak intensities (see Table 3) the well-prepared $NdPd_2Al_3$ PC1 sample shows no significant deviation from the ideal $PrNi_2Al_3$-type crystal structure.

The crystallographic unit cell of $NdPd_2Al_3$ contains only one magnetic Nd atom on site (1a) at (0, 0, 0). Concerning interatomic Nd–Nd distances at 14 K, Nd has two nearest neighbors at 4.20 Å (parallel to the c direction) and 6 second-nearest neighbors at 5.43 Å (inside the ab plane). The anisotropy of the thermal expansion of $NdPd_2Al_3$ is small, with the ratio of lattice parameters c/a increasing from 0.773 at room temperature to 0.774 at 14 K.

TABLE 2

Parameters of Crystal Structure at 14 K and of Magnetic Structure at 1.5 K of $NdPd_2Al_3$ (sample PC1), Obtained from FullProf Refinements of HRPD (BNL) Neutron Diffraction Data[a]

$NdPd_2Al_3$: crystal structure of 14 K

Space group: *P6/mmm* (No. 191)

Lattice parameters: $a = 5.427(3)$ Å, $c = 4.203(2)$ Å

Atom	Site	*x/a*	*y/a*	*z/c*	*B* (Å^2)
Nd	(1*a*)	0	0	0	0.13(11)
Pd	(2*c*)	1/3	2/3	0	0.38(12)
Al	(3*g*)	1/2	0	1/2	0.23(13)

$NdPd_2Al_3$: magnetic structure at 1.5 K

Propagation vector: $\mathbf{k} = [1/2, 0, 0]$

Atom	*x/a*	*y/a*	*z/c*	μ_x (μ_B)	μ_y (μ_B)	μ_z (μ_B)
Nd	0	0	0	0	2.28(7)	0

[a] The errors given for the lattice parameters include the estimated error of the neutron wavelength calibration.

The HRPD powder neutron diffraction pattern of $NdPd_2Al_3$ (sample PC1) recorded at 1.5 K is shown in Fig. 5b. The diffraction pattern contains additional Bragg peaks, which arise from scattering from the ordered magnetic moments of Nd ions. Magnetic lines of $NdPd_2Al_3$ can all be indexed by the propagation vector $\mathbf{k} = [1/2, 0, 0]$. The strongest magnetic intensity appears for the peak (1/2, 0, 0) at $2\theta = 11.5°$, whereas no magnetic intensity is observed for the reflection (1/2, −1, 0) at $2\theta = 20.0°$ (see Fig. 5b). Crystal and magnetic structures of $NdPd_2Al_3$ at 1.5 K were simultaneously analyzed by the FullProf program (22), based on a relativistic magnetic form factor for Nd^{3+} in dipolar approximation. A refinement of 14 inequivalent nuclear Bragg peaks and 27 inequivalent magnetic Bragg peaks in the scattering angle range $8° \leq 2\theta \leq 79°$ yielded the best fit ($\chi^2 = 2.57$) for the antiferromagnetic structure given in Table 2. Calculated and observed integrated magnetic neutron intensities are compared in Table 4. The agreement values of the FullProf fit were $R_{wp} = 11.4\%$, $R_{exp} = 7.12\%$, $R_{I,N} = 4.54\%$ (for integrated nuclear intensities) and $R_{I,M} = 16.3\%$ (for integrated magnetic intensities).

The antiferromagnetic structure of $NdPd_2Al_3$ is illustrated in Fig. 6. The ordered magnetic Nd moments of $(2.28 \pm 0.07)\ \mu_B$ at 1.5 K lie in the basal plane and are oriented perpendicular to the propagation vector **k**. At the magnetic phase transition of $NdPd_2Al_3$ the symmetry is lowered from hexagonal for the crystal structure (space group *P6/mmm*, No. 191) to orthorhombic for the magnetic structure (space group *Cmmm*, No. 65, with $a_{ortho} = \sqrt{3} \cdot a_{hex}$, $b_{ortho} = b_{hex}$, $c_{ortho} = c_{hex}$). A change in the description of the $NdPd_2Al_3$ crystal structure from hexagonal to orthorhombic implies a transformation of the hexagonal sites

Nd	(1*a*)	(0, 0, 0)	(*P6/mmm*)
Pd	(2*c*)	(1/3, 2/3, 0)	(*P6/mmm*)
Al	(3*g*)	(1/2, 0, 1/2)	(*P6/mmm*)

to the orthorhombic sites

Nd	(2*a*)	(0, 0, 0)	(*Cmmm*)
Pd	(4*g*)	(*x*, 0, 0)	(*Cmmm*)
		$x \approx 1/3$	
Al	(2*c*)	(1/2, 0, 1/2)	(*Cmmm*)
Al	(4*f*)	(1/4, 1/4, 1/2)	(*Cmmm*).

The antiferromagnetic structure of $NdPd_2Al_3$ may be

TABLE 3

Observed and Calculated Integrated Neutron Intensities of Paramagnetic $NdPd_2Al_3$ (Sample PC1) at 14 K[a]

h	*k*	*l*	2θ (deg)	I_{calc}	I_{obs}	(Δ)
1	0	0	23.15	15.0	6.1	(14.0)
0	0	1	25.93	121.2	112.6	(21.8)
1	0	1	35.03	132.7	149.1	(22.1)
1	1	0	40.67	465.2	428.2	(29.3)
2	0	0	47.31	205.9	230.5	(23.2)
1	1	1	48.86	1370.9	1398.4	(44.9)
0	0	2	53.31	332.9	350.0	(25.1)
2	0	1	54.73	154.3	147.8	(19.4)
1	0	2	58.87	4.6	10.0	(10.1)
2	1	0	64.12	3.9	4.7	(9.3)
1	1	2	69.15	381.2	386.1	(23.3)
2	1	1	70.37	84.6	94.4	(15.7)
3	0	0	74.01	173.4	193.4	(10.7)
2	0	2	74.01	206.0	229.9	(12.7)
3	0	1	79.93	643.9	660.8	(26.8)
0	0	3	84.59	15.7	19.4	(11.2)
2	2	0	88.05	489.8	501.5	(22.7)
2	1	2	88.05	4.6	4.7	(0.2)
1	0	3	89.21	32.7	29.2	(11.6)
3	1	0	92.66	2.1	4.4	(7.1)
2	2	1	93.82	85.1	99.6	(13.6)
3	0	2	97.30	257.5	268.0	(17.5)
3	1	1	98.46	61.3	68.1	(2.6)
1	1	3	98.47	526.2	585.3	(22.1)
2	0	3	103.16	67.6	83.2	(13.0)
4	0	0	106.74	75.1	77.9	(12.7)
2	2	2	111.63	849.7	862.6	(28.6)
4	0	1	112.87	65.5	69.8	(13.1)
3	1	2	116.68	3.4	3.2	(8.7)
2	1	3	117.98	60.6	51.2	(13.8)
3	2	0	121.97	1.7	7.2	(8.8)
0	0	4	127.60	150.8	171.1	(22.1)
3	2	1	129.06	65.8	63.2	(3.7)
3	0	3	129.07	539.6	524.8	(30.6)
4	1	0	133.67	275.1	288.8	(22.4)
4	0	2	133.67	172.3	181.4	(14.1)
1	0	4	133.68	1.8	1.9	(0.1)

[a] Estimated standard deviations corresponding to counting statistics are given in parentheses. The agreement value $R_{I,N} = \Sigma |I_{obs} - I_{calc}| / \Sigma I_{obs}$ results in 5.39%.

described either by the hexagonal unit cell (dashed lines in Fig. 6) and the propagation vector $\mathbf{k} = [1/2, 0, 0]$ or by the anticentered orthorhombic magnetic unit cell (marked by gray color in Fig. 6). A possible orthorhombic distortion of the $NdPd_2Al_3$ crystal structure below T_N is too small to be observed by the resolution of the neutron diffraction experiment.

The temperature dependence of magnetic Bragg peaks of $NdPd_2Al_3$ (sample PC1) was studied in the neutron powder diffraction experiment on the IN3 spectrometer ($\lambda = 2.36$ Å). The inset of Fig. 5c displays 2θ scans through the strongest magnetic peak (1/2, 0, 0) measured in the ordered state at 2 K and in the paramagnetic state of 10 K. The absence of magnetic intensity of the (1/2, −1, 0) reflection was confirmed at several temperatures between 1.5 and 14 K. Thus, the direction of the ordered Nd moments, as plotted in Fig. 6, is temperature independent below T_N, and the sublattice magnetization can be determined from the square root of the observed magnetic intensity of the (1/2, 0, 0) reflection. The magnetization

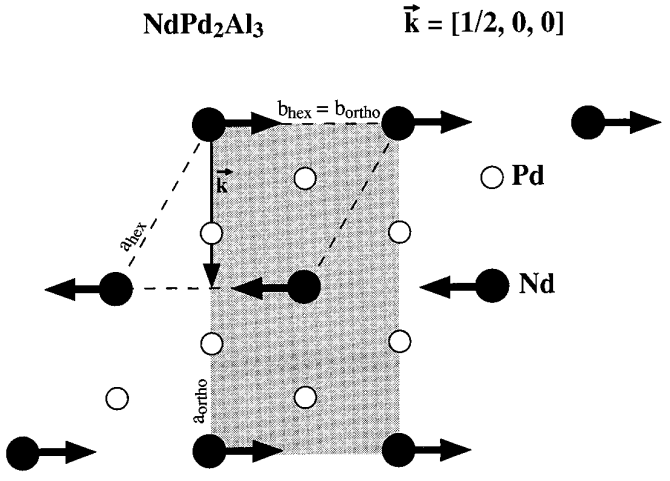

FIG. 6. Antiferromagnetic Nd moment arrangement of $NdPd_2Al_3$. The magnetic structure can be described either by the hexagonal unit cell (dashed lines) and the propagation vector **k** or by the anticentered orthorhombic magnetic unit cell marked by gray color.

TABLE 4
Observed and Calculated Magnetic Integrated Neutron Intensities of $NdPd_2Al_3$ (Sample PC1) at 1.5 K[a]

h	k	l	2θ (deg)	I_{calc}	I_{obs}	(Δ)
1/2	0	0	11.53	259.4	255.2	(32.4)
1/2	−1	0	20.03	0.0	0.0	(0.0)
1/2	0	1	28.48	82.0	103.6	(22.4)
1/2	1	0	30.81	39.8	53.2	(18.9)
1/2	−1	1	33.00	37.6	47.8	(18.0)
3/2	0	0	35.07	26.5	29.7	(3.8)
1/2	1	1	40.71	58.0	59.2	(3.3)
1/2	−2	0	42.45	2.8	7.4	(9.8)
3/2	0	1	44.14	32.6	38.8	(15.3)
1/2	−2	1	50.43	16.4	20.0	(12.1)
1/2	2	0	54.79	8.8	9.2	(0.8)
1/2	0	2	54.80	20.4	21.2	(2.0)
1/2	−1	2	57.58	15.8	23.6	(11.4)
3/2	1	1	58.94	30.4	31.2	(10.8)
5/2	0	0	60.27	8.3	3.2	(9.1)
1/2	2	1	61.60	16.8	28.4	(11.4)
3/2	−3	0	62.90	0.0	0.0	(0.0)
1/2	1	2	62.91	26.8	50.8	(12.5)
3/2	0	2	65.47	13.8	6.8	(9.9)
5/2	0	1	66.73	13.2	13.8	(10.1)
1/2	−3	0	67.99	1.6	0.0	(6.5)
3/2	−3	1	69.23	2.0	1.8	(0.1)
1/2	−2	2	70.46	14.8	15.6	(2.1)
1/2	−3	1	74.10	5.2	6.0	(0.3)
3/2	2	0	75.29	7.0	13.8	(9.0)
5/2	1	0	77.67	8.8	11.0	(3.9)
3/2	1	2	77.67	17.6	21.6	(7.8)

[a] The Bragg peaks are indexed with respect to the hexagonal chemical unit cell. Estimated standard deviations corresponding to counting statistics are given in parentheses. The agreement value $R_{I,M} = \sum |I_{obs} - I_{calc}| / \sum I_{obs}$ results in 16.3%.

curve, shown in Fig. 5c, indicates for the $NdPd_2Al_3$ PC1 sample a second-order phase transition with a Néel temperature $T_N = (7.7 \pm 0.1)$ K, in agreement with the anomalies of magnetic susceptibility and specific heat (see Fig. 2).

At 1.5 K the magnitude of the ordered Nd moments reaches the saturation value $\mu_0(\mathrm{Nd}) = 2.28(7)\ \mu_B$, which is reduced below the free ion value 3.27 μ_B of Nd^{3+} with $^4I_{9/2}$ ground state due to crystalline–electric field (CEF) effects. For the CEF ground-state doublet $\Gamma_7 = |\pm 1/2\rangle$ of $NdPd_2Al_3$ (21) the expected ordered moments are ($g_J = 8/11$)

$$\langle \mu_{a,b} \rangle = (1/2) \cdot (g \cdot \mu_B) \cdot \langle +1/2 | J^+ | - 1/2 \rangle = 1.82\ \mu_B$$

for the basal plane and

$$\langle \mu_c \rangle = (g \cdot \mu_B) \cdot \langle +1/2 | J^z | + 1/2 \rangle = 0.36\ \mu_B$$

parallel to the c axis. The large magnetic anisotropy induced by the Γ_7 CEF ground state fixes the directions of the ordered Nd moments into the basal plane as deduced from the neutron diffraction data. In $NdPd_2Al_3$ the strength of the magnetic exchange interactions ($T_N = 7.7$ K) is comparable to the energy separation ($\Delta E = 10$ K) of the two lowest-lying CEF doublets Γ_7 and $\Gamma_9^{(1)}$. Thus, the enhancement of the ordered moment $\mu_0(\mathrm{Nd}) = 2.28(7)\ \mu_B$ above the value 1.82 μ_B expected for Γ_7 reflects the mixing of $\Gamma_9^{(1)}$ into the ground-state singlet of the antiferromagnetically ordered state of $NdPd_2Al_3$.

4. CONCLUSIONS

We have presented a study on the sample dependence of magnetic properties and the determination of the antiferromagnetic structure of the ternary intermetallic com-

TABLE 5
Comparison of Magnetic Properties of the Compounds $CePd_2Al_3$, $NdPd_2Al_3$, UPd_2Al_3, $CePd_2Ga_3$, and $NdPd_2Ga_3$, All with Hexagonal $PrNi_2Al_3$-Type Crystal Structure[a]

Compound	$CePd_2Al_3$	$NdPd_2Al_3$	UPd_2Al_3	$CePd_2Ga_3$	$NdPd_2Ga_3$
References	(3, 4)	This work	(1, 2)	(25, 26)	(27)
a (Å)	5.4709	5.4419	5.365	5.4147	5.384
c (Å)	4.2156	4.2069	4.186	4.2607	4.247
c/a	0.7705	0.7731	0.780	0.7869	0.789
γ (mJ mol^{-1} K^{-2})	380	<20	150	>300	<20
T_{ord} (K)	$T_N = 2.8$	$T_N = 7.7$	$T_N = 14$	$T_C \approx 6$	$T_N = 6.5$
k	[0, 0, 1/2]	[1/2, 0, 0]	[0, 0, 1/2]	[0, 0, 0]	[1/2, 0, 0]
μ_0 (μ_B)	0.47(2)	2.28(7)	0.85(3)	1.5(1)	1.99(4)
	$\vec{\mu} \perp \mathbf{c}$	$\vec{\mu} \perp \mathbf{c}$	$\vec{\mu} \perp \mathbf{c}$	$\vec{\mu} \perp \mathbf{c}$	$\vec{\mu} \perp \mathbf{c}$
	$\vec{\mu} \perp \mathbf{k}$	$\vec{\mu} \perp \mathbf{k}$	$\vec{\mu} \perp \mathbf{k}$		$\vec{\mu} \perp \mathbf{k}$

[a] a, c, Room temperature lattice parameters; γ, electronic specific heat coefficient; T_{ord}, magnetic ordering temperature; **k**, magnetic propagation vector; μ_0, ordered magnetic saturation moment with direction $\vec{\mu}$.

pound $NdPd_2Al_3$ with ordered hexagonal $PrNi_2Al_3$-type crystal structure.

For a series of five selected polycrystalline and single-crystalline $NdPd_2Al_3$ samples we observe a significant dependence of physical properties [differences in the room temperature lattice parameters of up to 0.0032(2) Å for a and 0.0025(2) Å for c] and of magnetic properties (average Néel temperatures between 7.7 and 5.2 K) on sample preparation procedures. $NdPd_2Al_3$ samples of better quality (defined as structural perfection with respect to the ideal $PrNi_2Al_3$-type lattice) are characterized by smaller lattice parameters and higher values for the Néel temperature (see Table 1). The Néel temperature T_N shows a linear dependence on the lattice parameter a, which is not valid for c. A sample dependence has previously been reported for the heavy-fermion superconductor UPd_2Al_3 [the superconducting transition temperature T_c (9, 10)] and for the nonsuperconducting heavy-fermion antiferromagnet $CePd_2Al_3$ [the Néel temperature T_N (5)]. The present results on the non-heavy-fermion compound $NdPd_2Al_3$ suggests that such effects are intrinsic material properties that do not depend much on heavy-fermion properties. For the isostructural compounds $REPd_2Al_3$ (RE = U, Ce, Nd), well-prepared and annealed PC material, prepared by arc melting, is generally of better quality than SC material, prepared by the Czochralski pulling method. Limited sample quality of $REPd_2Al_3$ single crystals has been observed for RE = Nd at Néel temperatures much reduced below $T_N = 7.7$ K (see Table 1), for RE = Ce by the absence of long-range magnetic ordering (5), and for RE = U possibly by a small anomaly in the order parameter below T_N = 14 K (13–15). The difference in sample quality between SC and PC material seems to be caused by different amounts of material loss (evaporation of aluminum) during the process of sample preparation. As demonstrated for UPd_2Al_3 (10, 11), SC sample quality can be improved to some degree by choosing a nonstoichiometric (aluminum-rich) composition of the starting material. Efforts to improve the quality of $REPd_2Al_3$ single crystals are highly desirable, particularly for RE = Ce.

Our best $NdPd_2Al_3$ sample was investigated by high-resolution powder neutron diffraction. The antiferromagnetic structure below $T_N = 7.7$ K corresponds to a propagation vector **k** = [1/2, 0, 0]. The ordered magnetic Nd moments of (2.28 ± 0.07) μ_B at saturation lie in the basal plane due to CEF anisotropy and are oriented perpendicular to the propagation vector as illustrated in Fig. 6. Magnetic properties of the compounds $CePd_2Al_3$, $NdPd_2Al_3$, UPd_2Al_3, $CePd_2Ga_3$, and $NdPd_2Ga_3$, all with $PrNi_2Al_3$-type crystal structure, are compared in Table 5. The heavy-fermion antiferromagnet UPd_2Ga_3 (28) adopts a different (BaB_2Pt_3-type) crystal structure. Magnetic structures of the compounds in Table 5 are characterized by different propagation vectors (**k** = 0 for $CePd_2Ga_3$, **k** = [0, 0, 1/2] for $CePd_2Al_3$ and UPd_2Al_3, and **k** = [1/2, 0, 0] for $NdPd_2Al_3$ and $NdPd_2Ga_3$). It is remarkable that for all compounds the ordered magnetic moments are oriented perpendicular to the hexagonal c axis and perpendicular to the respective propagation vectors. CEF interactions of hexagonal symmetry induce strong magnetic anisotropies, which seem to favor the basal plane. There, the antiferromagnetic coupling of the ordered moments found for $NdPd_2Al_3$ and $NdPd_2Ga_3$ contrasts with the ferromagnetic coupling observed for $CePd_2Al_3$, $CePd_2Ga_3$, and UPd_2Al_3. It is interesting to note that for the Kondo compounds $YbCu_3Al_2$ (29) and $YbCu_{3.25}Al_{1.75}$ (30) the antiferromag-

netic Yb ordering corresponds to a similar propagation vector $\mathbf{k} = [1/2, 0, 0]$ with a different orientation parallel to the hexagonal c axis.

ACKNOWLEDGMENTS

We thank Professor K. Katsumata for the chance to use the SQUID magnetometer at the RIKEN Institute. Financial support by the Swiss National Science Foundation and the Paul Scherrer Institute is gratefully acknowledged.

REFERENCES

1. C. Geibel, C. Schank, S. Thies, H. Kitazawa, C. D. Bredl, A. Böhm, M. Rau, A. Grauel, R. Caspary, R. Helfrich, U. Ahlheim, G. Weber, and F. Steglich, *Z. Phys. B* **84,** 1 (1991).
2. A. Krimmel, P. Fischer, B. Roessli, H. Maletta, C. Geibel, C. Schank, A. Grauel, A. Loidl, and F. Steglich, *Z. Phys. B* **86,** 161 (1992).
3. H. Kitazawa, C. Schank, S. Thies, B. Seidel, C. Geibel, and F. Steglich, *J. Phys. Soc. Jpn.* **61,** 1461 (1992).
4. A. Dönni, P. Fischer, B. Roessli, and H. Kitazawa, *Z. Phys. B* **93,** 449 (1994).
5. S. A. M. Mentink, G. J. Nieuwenhuys, A. A. Menovsky, J. A. Mydosh, H. Tou, and Y. Kitaoka, *Phys. Rev. B* **49,** 15759 (1994).
6. J. Tang, A. Matsushita, H. Kitazawa, and T. Matsumoto, *Physica B* **217,** 97 (1996).
7. K. Ghosh, S. Ramakrishnan, S. K. Malik, and G. Chandra, *Phys. Rev. B* **48,** 6249 (1993).
8. H. Kitazawa, A. Mori, S. Takano, T. Yamadaya, A. Matsushita, and T. Matsumoto, *Physica B* **186–188,** 661 (1993).
9. E. Colineau, J. P. Sanchez, J. Rebizant, and J. M. Winand, *Solid State Commun.* **92,** 915 (1994).
10. N. Sato, T. Sakon, N. Takeda, T. Komatsubara, C. Geibel, and F. Steglich, *J. Phys. Soc. Jpn.* **61,** 32 (1992).
11. N. Sato, T. Sakon, K. Imamura, Y. Inada, H. Aono, and T. Komatsubara, *Physica B* **186–188,** 195 (1993).
12. L. Paolasini, R. Caciuffo, G. H. Lander, J. Reibizant, D. Keen, N. Sato, and T. Komatsubara, *J. Phys. Chem. Solids* **56,** 1323 (1995).
13. A. Grauel, A. Böhm, H. Fischer, C. Geibel, R. Köhler, R. Modler, C. Schank, F. Steglich, G. Weber, T. Komatsubara, and N. Sato, *Phys. Rev. B* **46,** 5818 (1992).
14. B. D. Gaulin, D. Gibbs, E. D. Isaacs, J. G. Lussier, J. N. Reimers, A. Schröder, L. Taillefer, and P. Zschack, *Phys. Rev. Lett.* **73,** 890 (1994).
15. H. Kita, A. Dönni, Y. Endoh, K. Kakurai, N. Sato, and T. Komatsubara, *J. Phys. Soc. Jpn.* **63,** 726 (1994).
16. A. Krimmel, P. Fischer, B. Roessli, C. Geibel, F. Steglich, and A. Loidl, *J. Magn. Magn. Mater.* **149,** 380 (1995).
17. S. A. M. Mentink, N. M. Bos, G. J. Nieuwenhuys, A. Drost, E. Frikkee, L. T. Tai, A. A. Menovsky, and J. A. Mydosh, *Physica B* **186–188,** 497 (1993).
18. H. Toroya, *J. Appl. Cystallogr.* **19,** 440 (1986).
19. J. D. Axe, S. Cheung, D. E. Cox, L. Passell, T. Vogt, and S. Bar-Ziv, *J. Neutron Res.* **2,** 85 (1994).
20. L. Passell, S. Bar-Ziv, D. W. Gardner, D. E. Cox, and J. D. Axe, *Mater. Sci. Forum* **79–82,** 475 (1991).
21. A. Dönni, and A. Furrer, unpublished results.
22. J. Rodriguez-Carvajal, *Physica B* **192,** 55 (1993).
23. V. F. Sears, *Neutron News* **3,** 26 (1992).
24. B. van Laar and W. B. Yelon, *J. Appl. Crystallogr.* **17,** 47 (1984).
25. E. Bauer, R. Hauser, E. Gratz, G. Schaudy, M. Rotter, A. Lindbaum, D. Gignoux, and D. Schmitt, *Z. Phys. B* **92,** 411 (1993).
26. E. Bauer, G. Schaudy, G. Hilscher, L. Keller, P. Fischer, and A. Dönni, *Z. Phys. B* **94,** 359 (1994).
27. E. Bauer, M. Liendl, L. Naber, D. Werner, G. Hilscher, A. Dönni, P. Fischer, F. Fauth, and M. Zolliker, to be published.
28. S. Süllow, B. Ludoph, B. Becker, G. J. Nieuwenhuys, A. A. Menovsky, J. A. Mydosh, S. A. M. Mentink, and T. E. Mason, *Phys. Rev. B* **52,** 12784 (1995).
29. E. Bauer, E. Gratz, L. Keller, P. Fischer, and A. Furrer, *Physica B* **186–188,** 608 (1993).
30. E. Bauer, and L. Keller, unpublished results.